



High-Fidelity Photonic Three-Degree-of-Freedom Hyperparallel Controlled-Phase-Flip Gate

Guan-Yu Wang¹ and Hai-Rui Wei^{2*}

¹College of Mathematics and Physics, Beijing University of Chemical Technology, Beijing, China, ²School of Mathematics and Physics, University of Science and Technology Beijing, Beijing, China

Encoding computing qubits in multiple degrees of freedom (DOFs) of a photonic system allows hyperparallel quantum computation to enlarge channel capacity with less quantum resource, and constructing high-fidelity hyperparallel quantum gates is always recognized as a fundamental prerequisite for hyperparallel quantum computation. Herein, we propose an approach for implementing a high-fidelity photonic hyperparallel controlled-phase-flip (CPF) gate working with polarization, spatial-mode, and frequency DOFs, through utilizing the practical interaction between the single photon and the diamond nitrogen vacancy (NV) center embedded in the cavity. Particularly, the desired output state of the gate without computation errors coming from the practical interaction is obtained, and the robust fidelity is guaranteed in the nearly realistic condition. Meanwhile, the requirement for the experimental realization of the gate is relaxed. In addition, this approach can be generalized to complete the high-fidelity photonic three-DOF hyperparallel CPF^N gate and parity-check gate. These interesting features may make the present scheme have potential for applications in the hyperparallel quantum computation.

Keywords: quantum computation, hyperparallel quantum gate, multiple degrees of freedom, high fidelity, photon

OPEN ACCESS

Edited by:

Qing Ai,
Beijing Normal University, China

Reviewed by:

Nana Zhang,
Chongqing University of Posts and
Telecommunications, China

Ping Zhou,
Guangxi University for Nationalities,
China

*Correspondence:

Hai-Rui Wei
hrwei@ustb.edu.cn

Specialty section:

This article was submitted to
Optics and Photonics,
a section of the journal
Frontiers in Physics

Received: 02 June 2022

Accepted: 20 June 2022

Published: 11 August 2022

Citation:

Wang G-Y and Wei H-R (2022) High-Fidelity Photonic Three-Degree-of-Freedom Hyperparallel Controlled-Phase-Flip Gate.
Front. Phys. 10:960078.
doi: 10.3389/fphy.2022.960078

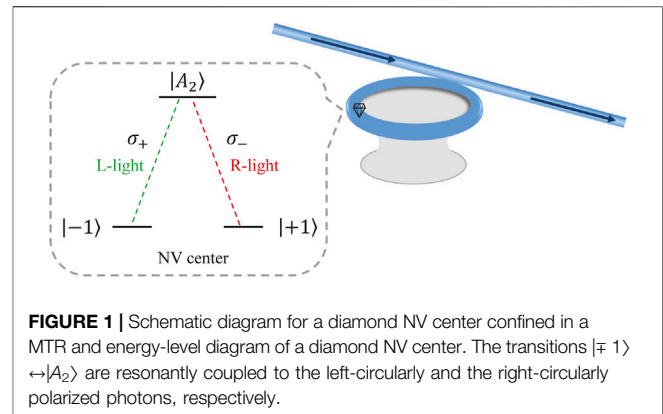
1 INTRODUCTION

Quantum information processing (QIP) which is accomplished based on quantum mechanics [1] surpasses classical information processing in terms of communication [2–14], computation [15–18], precision metrology [19], and machine learning [20–22]. Due to the capability of parallel computing, quantum computation exhibits a fascinating performance compared with the conventional computation which works with a serial pattern. For example, it has been suggested that quantum algorithms can largely speed up factorizing a large number [15] and searching data [16, 17], and greatly reduce the computational complexity of simulation [23, 24]. Quantum computation can be referred to as a succession of nontrivial critical single-qubit gates and two-qubit gates, such as controlled-NOT (CNOT) gate or the identical controlled-phase-flip (CPF) gate [25]. Nowadays, numerous works have been made on CNOT gates or CPF gates [26, 27]. Hyperparallel quantum computation, acting on more than one qubit-like degree of freedom (DOF) simultaneously, can achieve full potential of the parallel computation [28]. In 2013, Ren et al. [29] proposed the first scheme for the hyperparallel CNOT gate acting on the polarization and spatial DOFs simultaneously, and later in 2015 a polarization-spatial hyperparallel Toffoli gate was proposed [30]. Hyperparallel quantum gates have attracted much attention in recent years due to

their excellent properties. Up to now, some interesting protocols for implementing hyperparallel quantum gates have been proposed *via* photon-matter platforms [31–36], and the inevitable incomplete and imperfect photon-matter interactions are usually not taken into account.

Photon has been widely recognized as an especially promising physical architecture for implementing hyperparallel quantum gates due to its high transmitting speed, weak interaction with its environment, low cost for preparation, easy and accurate manipulation, and multiple qubit-like DOFs such as polarization, spatial mode, orbital angular momentum, time bin, and frequency [37–41]. It has been demonstrated that by encoding computing qubits in multiple DOFs of a photonic system, hyperparallel quantum gates can be achieved. The polarization and spatial-mode DOFs are particularly appealing for constructing photonic hyperparallel quantum gates [29–35]. For example, In 2014, Wang et al. [33] proposed an interesting scheme for implementing the hybrid hyperparallel CNOT gate, where the spatial-mode and polarization states of a photon control the two stationary electron spins in quantum dots simultaneously. In 2016, Wei et al. [34] constructed a hyperparallel Toffoli gate on a three-photon system in both the polarization and spatial-mode DOFs. Recently, frequency encoded photonic qubit has garnered much interest for its compatibility, stable in any transmission surroundings, and high-dimensional characters. In 2019, Lu et al. [42] demonstrated a frequency-bin based CNOT gate. And in 2020, Wei et al. [36] presented a hyperparallel CPF gate utilizing the frequency DOF together with the spatial-mode and time-bin DOFs of a two-photon system. Frequency-based entanglements were employed by Zeng and Zhu [43] to complete hyper-Bell analysis.

To achieve a deterministic (hyperparallel) quantum photonic gate, an essential prerequisite is obtaining the strong interactions between individual photons, which can be completed by employing cross-Kerr medium or cavity quantum electrodynamics (QED) with trapped atoms or artificial atoms (such as quantum dot, superconductor, diamond nitrogen vacancy (NV) center, Josephson junction). A diamond NV center is a promising candidate owing to its long-lived coherence time even at room temperature [44–48] and optical controllability including fast microwave manipulation, optical preparation, and read out [49–52]. Meanwhile, it has been experimentally realized the strong coupling between the NV center and the whispering-gallery mode (WGM) resonator [53–55], which can enhance the NV-photon interaction and the photon-photon interaction. In 2011, Chen et al. [56] introduced the interaction between the polarized single photon and the NV center confined in the WGM microtoroidal resonator (MTR). Utilizing the photon-NV interactions, where the realistic NV-cavity parameters are not taken into consideration, some interesting works on (hyperparallel) quantum gate have been presented [30, 35, 36, 57–59]. It is worthy to relax the necessary for high-Q cavity system, and to further improve the fidelity of the schemes in realistic environment by preventing the imperfect and incomplete photon-NV interactions. In 2012, by utilizing the practical interaction between the single photon and the atom-cavity system, Li et al. [60] proposed the robust-fidelity entangling gate in which the computation errors coming from



the realistic atom-cavity parameters were wiped out. In recent years, much attention has been attracted to the research in high-fidelity (hyperparallel) quantum gates *via* different methods [32, 61–71].

In this paper, through utilizing the practical interaction between a NV-cavity system and a single photon, we put forward a method for implementing a high-fidelity hyperparallel CPF gate working with three DOFs of a two-photon system. Here, the polarization-polarization-based, the spatial-spatial-based, and the frequency-frequency-based CPF gates are completed simultaneously, which is equal to three CPF gates operating simultaneously on the systems in one DOF, and the potential of parallel computation is further achieved. Particularly, the fidelity of this hyperparallel CPF gate is robust against the realistic NV-cavity parameters, since the computation errors coming from the practical interaction are wiped out by the single-photon detectors. This self-error-detected working pattern also relaxes the requirement for the experimental realization of the gate. In addition, the method can be generalized to achieve the high-fidelity photonic hyperparallel CPF^N gate and parity-check gate working on three DOFs. We use the frequency, spatial-mode, and polarization DOFs to complete our schemes, where a frequency encoded photonic qubit is naturally stable in the transmission surroundings as its alteration requires a nonlinear interaction between photon and an optical fiber, which takes place with a negligible probability, a spatial-mode encoded photonic qubit is robust against the bit-flip channel noise, and a polarization encoded photonic qubit can be skillfully manipulated. These interesting features may make our scheme more useful in the practical quantum computation tasks.

2 NONLINEAR INTERACTION BETWEEN A SINGLE PHOTON AND A DIAMOND NV CENTER INSIDE A MICROTOROIDAL RESONATOR

The nonlinear interaction between a single photon and a diamond NV center inside a microtoroidal resonator (MTR) which is employed as the platform for implementing our

hyperparallel CPF gate is illustrated in **Figure 1**. The ground state of a negatively charged diamond NV center is a spin triplet, and there exists 2.88 GHz zero-field splitting between levels $|0\rangle$ with $m_s = 0$ and $|\pm 1\rangle$ with $m_s = \pm 1$ owing to spin-spin interactions. There exist six excited states defined by the group theory as $|A_1\rangle = |E_-\rangle|+1\rangle - |E_+\rangle|-1\rangle$, $|A_2\rangle = |E_-\rangle|+1\rangle + |E_+\rangle|-1\rangle$, $|E_x\rangle = |X\rangle|0\rangle$, $|E_y\rangle = |Y\rangle|0\rangle$, $|E_1\rangle = |E_-\rangle|-1\rangle - |E_+\rangle|+1\rangle$, and $|E_2\rangle = |E_-\rangle|-1\rangle + |E_+\rangle|+1\rangle$, which are eigenstates of the full Hamiltonian including spin-orbit and spin-spin interactions in the absence of any perturbation [72]. Here, $|E_-\rangle$, $|E_+\rangle$, $|X\rangle$, and $|Y\rangle$ are orbital states. $|A_1\rangle$ and $|A_2\rangle$ are split from the other excited states by at least 5.5 GHz due to the spin-orbit interaction, and the energy gap between these two states is increased to 3.3 GHz due to spin-spin interaction [56, 72]. Thus, in the limit of low strain and magnetic field, the excited state $|A_2\rangle$ is robust against the stable symmetric properties and preserves the polarization properties of its optical transitions to states $|\pm 1\rangle$ through polarized radiations $|\sigma_{\mp}\rangle$ due to total angular momentum conservations. That is to say, as shown in **Figure 1**, the two transitions $|A_2\rangle \leftrightarrow |\pm 1\rangle$ are resonantly coupled to the right- and the left-circularly polarized photons with the identical transition frequency ω_0 , respectively.

After a circularly polarized single photon with frequency ω_p interacting with a NV-cavity system with mode frequency ω_c , it will be scattered with a reflection coefficient. In the weak excitation limit with the NV center predominantly in the ground state, through solving the Heisenberg equations of motion and the input-output relations, we can obtain the reflection coefficient as [73, 74]

$$r(\omega_p) = \frac{[i(\omega_0 - \omega_p) + \frac{\gamma}{2}][i(\omega_c - \omega_p) - \frac{\kappa}{2} + \frac{\kappa_s}{2}] + g^2}{[i(\omega_0 - \omega_p) + \frac{\gamma}{2}][i(\omega_c - \omega_p) + \frac{\kappa}{2} + \frac{\kappa_s}{2}] + g^2}, \quad (1)$$

where κ and κ_s are the cavity damping rate and the side-leakage rate, respectively. γ is the NV center dipolar decay rate, and g is the coupling strength between the cavity and the NV center. By taking $g = 0$, the reflection coefficient for a cold cavity (i.e., the NV center is uncoupled to the cavity) is obtained as

$$r'(\omega_p) = \frac{i(\omega_c - \omega_p) - \frac{\kappa}{2} + \frac{\kappa_s}{2}}{i(\omega_c - \omega_p) + \frac{\kappa}{2} + \frac{\kappa_s}{2}}. \quad (2)$$

Considering the single photon with frequency $\omega_p = \omega_1 \neq \omega_0$ being injected into the NV-cavity system with $\omega_c = \omega_0$, no matter what the polarization of the photon is or what the spin of the NV center is, the single photon always senses a cold cavity due to a large detuning and then it will be scattered with a reflection coefficient of $r'_1 = r'(\omega_1) = [2i(\omega_c - \omega_1) - \kappa + \kappa_s]/[2i(\omega_c - \omega_1) + \kappa + \kappa_s]$. However, when the single photon with frequency $\omega_p = \omega_2 = \omega_0$ is injected into the NV-cavity system with $\omega_c = \omega_0$, if the NV center is initially prepared in the state $|-1\rangle$, the single photon in the left-polarization state $|L\rangle$ feels a hot cavity and then obtains a reflection coefficient of $r_2 = r(\omega_2) = [\gamma(\kappa_s - \kappa) + 4g^2]/[\gamma(\kappa_s + \kappa) + 4g^2]$ after being scattered, whereas the single photon in the right-polarization state $|R\rangle$ experiences a cold cavity due to a polarization mismatch and then introduces a reflection coefficient of $r'_2 = r'(\omega_2) = (\kappa_s - \kappa)/(\kappa_s + \kappa)$ after being

scattered. Conversely, if the NV center is initially prepared in the state $|+1\rangle$, the $|R\rangle$ -polarized photon suffers a hot cavity and gets a reflection coefficient of r_2 after being scattered, whereas $|L\rangle$ -polarized photon experiences a cold cavity and gets a reflection coefficient of r'_2 after being scattered. Here, the reflection coefficients r'_1 , r'_2 , and r_2 are the functions of the realistic NV-cavity parameters. Therefore, the practical interaction rules, dependent on the polarization and frequency of the incident single photon and the spin of the NV center, can be summarized as

$$\begin{aligned} |L\rangle|\omega_1\rangle|+1\rangle &\rightarrow r'_1|L\rangle|\omega_1\rangle|+1\rangle, & |L\rangle|\omega_1\rangle|-1\rangle &\rightarrow r'_1|L\rangle|\omega_1\rangle|-1\rangle, \\ |R\rangle|\omega_1\rangle|+1\rangle &\rightarrow r'_1|R\rangle|\omega_1\rangle|+1\rangle, & |R\rangle|\omega_1\rangle|-1\rangle &\rightarrow r'_1|R\rangle|\omega_1\rangle|-1\rangle, \\ |L\rangle|\omega_2\rangle|+1\rangle &\rightarrow r'_2|L\rangle|\omega_2\rangle|+1\rangle, & |L\rangle|\omega_2\rangle|-1\rangle &\rightarrow r_2|L\rangle|\omega_2\rangle|-1\rangle, \\ |R\rangle|\omega_2\rangle|+1\rangle &\rightarrow r_2|R\rangle|\omega_2\rangle|+1\rangle, & |R\rangle|\omega_2\rangle|-1\rangle &\rightarrow r_2|R\rangle|\omega_2\rangle|-1\rangle. \end{aligned} \quad (3)$$

3 HIGH-FIDELITY PHOTONIC THREE-DOF HYPERPARALLEL CPF GATE

Based on the practical interaction between the single photon and the NV-cavity system as described in **Eq. 3**, we propose a scheme for implementing a high-fidelity photonic three-DOF hyperparallel CPF gate, in which the qubits are independently encoded in the frequency, polarization, and spatial-mode DOFs of the single photons. Suppose the control photon a , the target photon b , and the three NV centers are initially prepared in the normalized states

$$\begin{aligned} |\phi\rangle_a &= (\alpha_1|F\rangle + \alpha_2|S\rangle) \otimes (\beta_1|\omega_1\rangle + \beta_2|\omega_2\rangle) \otimes (\gamma_1|a_1\rangle + \gamma_2|a_2\rangle), \\ |\phi\rangle_b &= (\delta_1|F\rangle + \delta_2|S\rangle) \otimes (\eta_1|\omega_1\rangle + \eta_2|\omega_2\rangle) \otimes (\xi_1|b_1\rangle + \xi_2|b_2\rangle), \\ |\phi\rangle_1 &= |+\rangle_1, \quad |\phi\rangle_2 = |+\rangle_2, \quad |\phi\rangle_3 = |+\rangle_3. \end{aligned} \quad (4)$$

Here and afterwards, $|\pm\rangle = \frac{1}{\sqrt{2}}(|+1\rangle \pm |-1\rangle)$ are the states of the NV centers; $|F\rangle = \frac{1}{\sqrt{2}}(|R\rangle + |L\rangle)$ and $|S\rangle = \frac{1}{\sqrt{2}}(|R\rangle - |L\rangle)$ are the polarization states of the single photons; $|\omega_1\rangle$ and $|\omega_2\rangle$ are the frequency states of the single photons; $|a_1\rangle$, $|a_2\rangle$, $|b_1\rangle$, and $|b_2\rangle$ are the spatial-mode states of the single photons.

The photonic hyperparallel CPF gate in three DOFs completes the task that when the polarization state of photon a is $|S\rangle$, a phase flip takes place on the polarization state $|S\rangle$ of photon b , when the spatial-mode state of photon a is $|a_2\rangle$, a phase flip takes place on the spatial-mode state $|b_2\rangle$ of photon b , and when the frequency state of photon a is $|\omega_2\rangle$, a phase flip takes place on the frequency state $|\omega_2\rangle$ of photon b , simultaneously. The quantum circuit for implementing the three-DOF hyperparallel CPF gate is shown in **Figure 2**, and the principle is described in detail as follows in step by step.

Firstly, the control photon a is injected into the circuit from the input ports a_1 and a_2 . Through the circularly polarizing beam splitters (CPBSs), the wave packets in $|F\rangle$ are transmitted to the paths a_{11} and a_{21} for interacting with the NV₁-cavity system directly. Whereas the wave

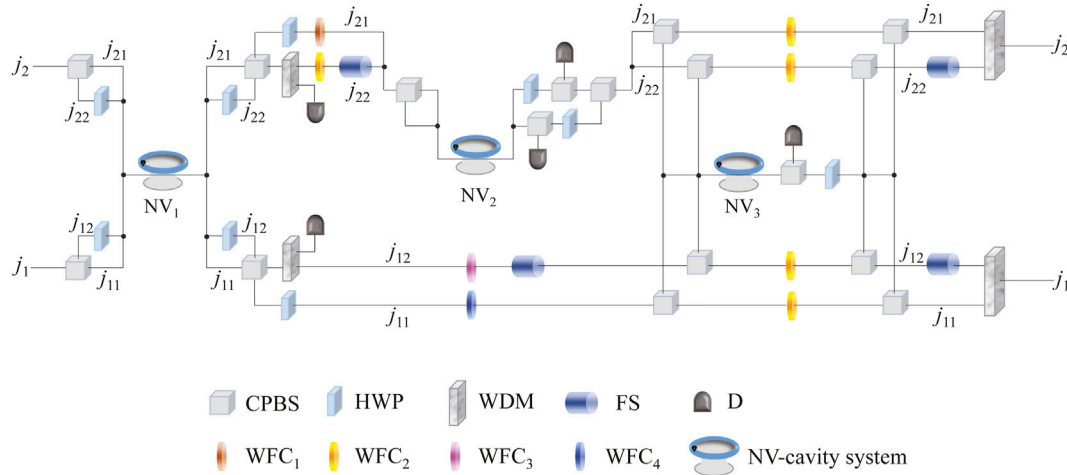


FIGURE 2 | Schematic diagram for implementing the high-fidelity photonic three-DOF hyperparallel CPF gate. j_1 and j_2 , where $j = a, b$, are the input ports for the control photon a and the target photon b being injected to the circuit in sequence. CPBS represents a circularly polarizing beam splitter in the basis $\{|F\rangle, |S\rangle\}$ transmitting the $|F\rangle$ -polarized photon and reflecting the $|S\rangle$ -polarized photon. HWP is a half-wave plate set at 0° performing operation $|F\rangle \leftrightarrow |S\rangle$. WFC $_i$ ($i = 1, 2, 3, 4$) represent wave-form corrector introducing coefficients r'_1 , $(r_2 - r'_2)/2$, $(r_2 - r'_2)^2/4$, and $r'_1(r_2 - r'_2)/2$ on the incident photons, respectively. WDM represents a polarization-independent wavelength division multiplexer, which divides photon with different frequencies from one path to different paths or completes the reverse conversion. FS is a frequency shifter which can shift the frequency ω_1 to ω_2 . D is a single-photon detector.

packets in $|S\rangle$ are reflected to the paths a_{12} and a_{22} , pass through the half plate waves (HWPs) resulting in $|F\rangle \leftrightarrow |S\rangle$, and interact with the NV $_1$ -cavity system. In this process, the wave packets in the four paths are respectively routed to interact with the NV $_1$ -cavity system. Then after the wave packets in the paths a_{12} and a_{22} pass through the HWPs, they reunite with the wave packets in the paths a_{11} and a_{21} at the CPBSs, and the state of the system is changed from

$$|\Phi\rangle_0 = |\phi\rangle_a \otimes |\phi\rangle_b \otimes |\phi\rangle_1 \otimes |\phi\rangle_2 \otimes |\phi\rangle_3 \quad (5)$$

to

$$|\Phi\rangle_1 = \left[\frac{r_2 - r'_2}{2} (\alpha_1 \beta_2 |S\rangle |\omega_2\rangle + \alpha_2 \beta_2 |F\rangle |\omega_2\rangle) |-\rangle_1 (\gamma_1 |a_{11}\rangle + \gamma_2 |a_{21}\rangle) \right. \\ \left. + \frac{r_2 + r'_2}{2} (\alpha_1 \beta_2 |F\rangle |\omega_2\rangle + \alpha_2 \beta_2 |S\rangle |\omega_2\rangle) |+\rangle_1 (\gamma_1 |a_{12}\rangle + \gamma_2 |a_{22}\rangle) \right]_a \\ \otimes |\phi\rangle_b \otimes |\phi\rangle_2 \otimes |\phi\rangle_3. \quad (6)$$

The wave packets in the path a_{21} pass through the HWP and the wave-form corrector $_1$ (WFC $_1$); the wave packets in the path a_{22} first pass through the wavelength division multiplexer (WDM), which divides photon with different frequencies to the different paths. If the wave packets in the path a_{22} are in the frequency states $|\omega_2\rangle$, they will trigger the single-photon detector which represents the process of the photonic hyperparallel CPF gate is terminated. Otherwise, the wave packets in the path a_{22} with frequency states $|\omega_1\rangle$ will pass through the WFC $_2$ and the frequency

shifter (FS) which shifts the frequency ω_1 to ω_2 ; Similarly, the wave packets in the path a_{12} pass through the WDM. If the wave packets in the path a_{12} are in the frequency states $|\omega_2\rangle$, they will trigger the single-photon detector which means the process of the hyperparallel CPF gate is terminated. Otherwise, the wave packets in the path a_{12} with frequency states $|\omega_1\rangle$ pass through the WFC $_3$ and the FS which shifts the frequency ω_1 to ω_2 ; the wave packets in the path a_{11} pass through the HWP and the WFC $_4$. Before the wave packets in the paths a_{21} and a_{22} passing through the CPBSs, the state of the system becomes

$$|\Phi\rangle_2 = \left[\frac{r'_1 (r_2 - r'_2)^2}{4} \beta_2 \gamma_1 (\alpha_1 |F\rangle + \alpha_2 |S\rangle) |\omega_2\rangle |-\rangle_1 |a_{11}\rangle \right. \\ \left. + \frac{r'_1 (r_2 - r'_2)^2}{4} \beta_1 \gamma_1 (\alpha_1 |F\rangle + \alpha_2 |S\rangle) |\omega_2\rangle |+\rangle_1 |a_{12}\rangle \right. \\ \left. + \frac{r'_1 (r_2 - r'_2)^2}{2} \beta_2 \gamma_2 (\alpha_1 |F\rangle + \alpha_2 |S\rangle) |\omega_2\rangle |-\rangle_1 |a_{21}\rangle \right. \\ \left. + \frac{r'_1 (r_2 - r'_2)^2}{2} \beta_1 \gamma_2 (\alpha_1 |F\rangle + \alpha_2 |S\rangle) |\omega_2\rangle |+\rangle_1 |a_{22}\rangle \right]_a \\ \otimes |\phi\rangle_b \otimes |\phi\rangle_2 \otimes |\phi\rangle_3. \quad (7)$$

Then, for the wave packets of photon a in the spatial-mode states $|a_2\rangle$, after they passing through the CPBS, the wave packets in the polarization states $|F\rangle$ interact with NV $_2$ -cavity system, pass through the HWP and the CPBS in sequence, and the wave packets in the polarization states $|S\rangle$ interact with NV $_2$ -cavity system, pass through the CPBS and the HWP in sequence. If either of the two single-photon detectors is clicked, the process of the hyperparallel

TABLE 1 | The relations between the measurement results on the NV centers and the feed-forward operations for completing a deterministic hyperparallel CPF gate working with the three DOFs of a two-photon system.

Measurement NV Center	Feed-Forward Operation	
	Control Photon	Target Photon
$ +\rangle_1$ (frequency)	none	none
$ -\rangle_1$ (frequency)	σ_{zf}	none
$ +\rangle_2$ (spatial mode)	none	none
$ -\rangle_2$ (spatial mode)	σ_{zs}	none
$ +\rangle_3$ (polarization)	none	none
$ -\rangle_3$ (polarization)	σ_{zp}	none

photonic CPF gate is terminated. If there is no click of the two single-photon detectors, the process continues, that is, the two wave packets of different polarizations in the spatial-mode states $|a_2\rangle$ reunite at the CPBS and the state of the system is changed into

$$|\Phi\rangle_3 = \frac{r'_1(r_2 - r'_2)^2}{4} [(\alpha_1|F\rangle + \alpha_2|S\rangle)(\beta_2\gamma_1|\omega_2\rangle - \gamma_1|a_{11}\rangle + \gamma_2 + \beta_1\gamma_1|\omega_2\rangle + \gamma_1|a_{12}\rangle + \gamma_2 + \beta_2\gamma_2|\omega_2\rangle - \gamma_1|a_{21}\rangle - \gamma_2 + \beta_1\gamma_2|\omega_2\rangle + \gamma_1|a_{22}\rangle - \gamma_2]_a \otimes |\phi\rangle_b \otimes |\phi\rangle_3. \quad (8)$$

Next, after photon a passing through the CPBSs, in the path $a_{11}(a_{12}, a_{21}, a_{22})$, the wave packets in the polarization states $|F\rangle$ pass through the WFC₂, and the wave packets in the polarization states $|S\rangle$ interact with NV₃-cavity system and pass through the CPBS. Similarly, if there is a click of the single-photon detector, the process of the high-fidelity hyperparallel photonic CPF gate is terminated. Otherwise, the process continues, that is, the polarization states of wave packets will be changed into $|S\rangle$ with the operation performed by HWP, which will unite with wave packets in the polarization states $|F\rangle$ at the CPBS. At this time, the state of the system becomes

$$|\Phi\rangle_4 = \frac{r'_1(r_2 - r'_2)^3}{8} [(\alpha_1|F\rangle + \gamma_3 + \alpha_2|S\rangle - \gamma_3)(\beta_2\gamma_1|\omega_2\rangle - \gamma_1|a_{11}\rangle + \gamma_2 + \beta_1\gamma_1|\omega_2\rangle + \gamma_1|a_{12}\rangle + \gamma_2 + \beta_2\gamma_2|\omega_2\rangle - \gamma_1|a_{21}\rangle - \gamma_2 + \beta_1\gamma_2|\omega_2\rangle + \gamma_1|a_{22}\rangle - \gamma_2]_a \otimes |\phi\rangle_b. \quad (9)$$

Subsequently, the wave packets in the paths a_{12} and a_{22} pass through the FSs which shift frequency ω_2 to ω_1 , and the wave packets in the paths a_{11} and a_{21} respectively unite with the wave packets in the paths a_{12} and a_{22} to the spatial modes $|a_1\rangle$ and $|a_2\rangle$ by the WDMs. At this time, the system composed of two photons and the three NV centers is changed into

$$|\Phi\rangle_5 = \frac{r'_1(r_2 - r'_2)^3}{8} [(\alpha_1|F\rangle + \gamma_3 + \alpha_2|S\rangle - \gamma_3)(\beta_1|\omega_1\rangle + \gamma_1 + \beta_2|\omega_2\rangle - \gamma_1)(\gamma_1|a_1\rangle + \gamma_2 + \gamma_2|a_2\rangle - \gamma_2)]_a \otimes |\phi\rangle_b. \quad (10)$$

Secondly, Hadamard operations $[|+\rangle \leftrightarrow |-\rangle, |-\rangle \leftrightarrow |+\rangle]$ are performed on the three NV centers, where the Hadamard operation can be implemented with a $\pi/2$ microwave pulse, and the state $|\Phi\rangle_5$ is changed into

$$|\Phi\rangle_6 = \frac{r'_1(r_2 - r'_2)^3}{8} [(\alpha_1|F\rangle + \gamma_3 + \alpha_2|S\rangle - \gamma_3)(\beta_1|\omega_1\rangle + \gamma_1 + \beta_2|\omega_2\rangle - \gamma_1)(\gamma_1|a_1\rangle + \gamma_2 + \gamma_2|a_2\rangle - \gamma_2)]_a \otimes |\phi\rangle_b. \quad (11)$$

Thirdly, the target photon b is injected into the circuit from the input ports b_1 and b_2 . After the same operations as those performed on the control photon a are applied on the target photon b , if none of the five single-photon detectors is clicked, the system will collapse into the state

$$|\Phi\rangle_7 = \frac{r'^2_1(r_2 - r'_2)^6}{64} [\beta_1|\omega_1\rangle_a + \gamma_1(\eta_1|\omega_1\rangle + \eta_2|\omega_2\rangle)_b + \beta_2|\omega_2\rangle_a - \gamma_1(\eta_1|\omega_1\rangle - \eta_2|\omega_2\rangle)_b] \otimes [\gamma_1|a_1\rangle + \gamma_2(\xi_1|b_1\rangle + \xi_2|b_2\rangle) + \gamma_2|a_2\rangle - \gamma_2(\xi_1|b_1\rangle - \xi_2|b_2\rangle)] \otimes [\alpha_1|F\rangle_a + \gamma_3(\delta_1|F\rangle + \delta_2|S\rangle)_b + \alpha_2|S\rangle_a - \gamma_3(\delta_1|F\rangle - \delta_2|S\rangle)_b]. \quad (12)$$

Finally, the three NV centers are measured in the orthogonal basis $\{|\pm\rangle\}$. According to **Table 1**, some feed-forward operations are performed on the control photon a . In detail, if NV₁ center is in the state $|-\rangle_1$, a frequency-based operation $\sigma_{zf} = |\omega_1\rangle\langle\omega_1| - |\omega_2\rangle\langle\omega_2|$ is performed on the control photon a ; if NV₂ center is in the state $|-\rangle_2$, a spatial-based operation $\sigma_{zs} = |a_1\rangle\langle a_1| - |a_2\rangle\langle a_2|$ is performed on the control photon a ; if NV₃ center is in the state $|-\rangle_3$, a polarization-based operation $\sigma_{zp} = |F\rangle\langle F| - |S\rangle\langle S|$ is performed on the control photon a . Conditioned on the results of the measurement on the three NV centers, the two-photon system collapses into the state

$$|\Phi\rangle_8 = \frac{r'^2_1(r_2 - r'_2)^6}{64} [\alpha_1|F\rangle_a(\delta_1|F\rangle + \delta_2|S\rangle)_b + \alpha_2|S\rangle_a(\delta_1|F\rangle - \delta_2|S\rangle)_b] \otimes [\beta_1|\omega_1\rangle_a(\eta_1|\omega_1\rangle + \eta_2|\omega_2\rangle)_b + \beta_2|\omega_2\rangle_a(\eta_1|\omega_1\rangle - \eta_2|\omega_2\rangle)_b] \otimes [\gamma_1|a_1\rangle(\xi_1|b_1\rangle + \xi_2|b_2\rangle) + \gamma_2|a_2\rangle(\xi_1|b_1\rangle - \xi_2|b_2\rangle)]. \quad (13)$$

From **Eq. 13**, one can see that a photonic three-DOF hyperparallel CPF gate is completed, in which the conditional phase flips take place on the states $|S\rangle_a|S\rangle_b$, $|\omega_2\rangle_a|\omega_2\rangle_b$, and $|a_2\rangle|b_2\rangle$, simultaneously. Notably, this hyperparallel CPF gate is locally equivalent to the hyperparallel quantum CNOT gate up to Hadamard operations performed on the target photon b .

Fidelity, which can characterize the performance of a quantum gate, is described by $F = |\langle\Psi_r|\Psi_i\rangle|^2$, where $|\Psi_i\rangle$ and $|\Psi_r\rangle$ are the ideal desired output state and realistic output state, respectively. From **Eq. 13**, one can see that there are no error items and the

only difference between the ideal desired output state and the realistic output state is the global coefficient $r_1^2(r_2 - r_2')^6/64$, which would not affect the fidelity. That is to say, the fidelity of the hyperparallel CPF gate is robust, which is immune to the realistic NV-cavity parameters including the damping rate κ , the side-leakage rate κ_s , the dipolar decay rate γ , and the coupling strength g . Overall, the quantum circuit shown in **Figure 2** implements a high-fidelity hyperparallel CPF gate in the frequency, spatial-mode, and polarization DOFs, simultaneously.

4 HIGH-FIDELITY PHOTONIC THREE-DOF HYPERPARALLEL CPF^N GATE AND PARITY CHECK GATE

The quantum circuit shown in **Figure 2** can be generalized to implement a high-fidelity hyperparallel CPF^N gate working with a multiple-photon system in the frequency, spatial-mode, and polarization DOFs. Initially, the three NV centers are also prepared in the states $|\phi\rangle_1 = |+\rangle_1$, $|\phi\rangle_2 = |+\rangle_2$, and $|\phi\rangle_3 = |+\rangle_3$. The control photon a is also initially prepared in the normalized arbitrary state

$$|\phi\rangle_a = (\alpha_1|F\rangle + \alpha_2|S\rangle)_a (\beta_1|\omega_1\rangle + \beta_2|\omega_2\rangle)_a (\gamma_1|a_1\rangle + \gamma_2|a_2\rangle)_a. \quad (14)$$

The N target photons $b^n (n = 1, 2, \dots, N)$ are initially prepared in the normalized arbitrary state

$$|\phi\rangle_{b^n} = (\delta_1^n|F\rangle + \delta_2^n|S\rangle)_{b^n} (\eta_1^n|\omega_1\rangle + \eta_2^n|\omega_2\rangle)_{b^n} (\xi_1^n|b_1\rangle + \xi_2^n|b_2\rangle)_{b^n}. \quad (15)$$

The procedure of the hyperparallel CPF^N gate completed with the quantum circuit shown in **Figure 2** is similar with that of the hyperparallel CPF gate described above but the target photon b is substituted with the target photon string b^1, b^2, \dots, b^N , which are injected into the quantum circuit in sequence.

Firstly, the control photon a is injected into the quantum circuit. While the photon a passes through the circuit, if any of the single-photon detectors is clicked, the construction process of the hyperparallel CPF^N gate is terminated. If there is no click of any single-photon detectors, the process goes on and with Hadamard operations respectively performed on the three NV centers, the state of the whole system is changed from $|\Phi^N\rangle_0$ to $|\Phi^N\rangle_1$, where

$$\begin{aligned} |\Phi^N\rangle_0 &= |\phi\rangle_a \otimes |\phi\rangle_{b^1} \otimes \dots \otimes |\phi\rangle_{b^N} \otimes |\phi\rangle_1 \otimes |\phi\rangle_2 \otimes |\phi\rangle_3, \\ |\Phi^N\rangle_1 &= \frac{r_1'(r_2 - r_2')^3}{8} [(\alpha_1|F\rangle + 1\rangle_3 + \alpha_2|S\rangle - 1\rangle_3)(\beta_1|\omega_1\rangle + 1\rangle_1 \\ &\quad + \beta_2|\omega_2\rangle - 1\rangle_1) \otimes (\gamma_1|a_1\rangle + 1\rangle_2 + \gamma_2|a_2\rangle - 1\rangle_2)]_a \\ &\quad \otimes |\phi\rangle_{b^1} \otimes \dots \otimes |\phi\rangle_{b^N}. \end{aligned} \quad (16)$$

Secondly, the first target photon b^1 is injected into the circuit. Similarly, while the photon b^1 passes through the circuit, if any of the single-photon detectors is clicked, the

construction process of the hyperparallel CPF^N gate is terminated. If none of any single-photon detector is clicked, the process of the hyperparallel CPF^N goes on and the state of the whole system becomes

$$\begin{aligned} |\Phi^N\rangle_2 &= \frac{r_1^2(r_2 - r_2')^6}{64} [\beta_1|+1\rangle_1|\omega_1\rangle_a (\eta_1^1|\omega_1\rangle + \eta_2^1|\omega_2\rangle)_{b^1} \\ &\quad + \beta_2|+1\rangle_1|\omega_2\rangle_a (\eta_1^1|\omega_1\rangle - \eta_2^1|\omega_2\rangle)_{b^1}] \\ &\quad \otimes [\gamma_1|+1\rangle_2|a_1\rangle_a (\xi_1^1|b_1\rangle + \xi_2^1|b_2\rangle)_{b^1} + \gamma_2|+1\rangle_2|a_2\rangle_a \\ &\quad (\xi_1^1|b_1\rangle - \xi_2^1|b_2\rangle)_{b^1}] \otimes [\alpha_1|+1\rangle_3|F\rangle_a (\delta_1^1|F\rangle + \delta_2^1|S\rangle)_{b^1} \\ &\quad + \alpha_2|+1\rangle_3|S\rangle_a (\delta_1^1|F\rangle - \delta_2^1|S\rangle)_{b^1}]. \end{aligned} \quad (17)$$

Subsequently, the target photons b^2, \dots, b^N are injected into the quantum circuit in sequence. Similarly, if any of the single-photon detector is clicked, the process is terminated. Otherwise, the process goes on. Then the state of the whole system is expressed as

$$\begin{aligned} |\Phi^N\rangle_3 &= P^{1+N} [|+1\rangle_1\beta_1|\omega_1\rangle_a (\eta_1^1|\omega_1\rangle + \eta_2^1|\omega_2\rangle)_{b^1} (\eta_1^2|\omega_1\rangle \\ &\quad + \eta_2^2|\omega_2\rangle)_{b^2} \dots (\eta_1^N|\omega_1\rangle + \eta_2^N|\omega_2\rangle)_{b^N} + |-1\rangle_1\beta_2|\omega_2\rangle_a (\eta_1^1|\omega_1\rangle \\ &\quad - \eta_2^1|\omega_2\rangle)_{b^1} (\eta_2^N|\omega_1\rangle - \eta_2^N|\omega_2\rangle)_{b^2} \dots (\eta_1^N|\omega_1\rangle - \eta_2^N|\omega_2\rangle)_{b^N}] \\ &\quad \otimes [|+1\rangle_2\gamma_1|a_1\rangle_a (\xi_1^1|b_1\rangle + \xi_2^1|b_2\rangle)_{b^1} (\xi_1^2|b_1\rangle \\ &\quad + \xi_2^2|b_2\rangle)_{b^2} \dots (\xi_1^N|b_1\rangle + \xi_2^N|b_2\rangle)_{b^N} + |-1\rangle_2\gamma_2|a_2\rangle_a (\xi_1^1|b_1\rangle \\ &\quad - \xi_2^1|b_2\rangle)_{b^1} (\xi_2^2|b_1\rangle - \xi_2^2|b_2\rangle)_{b^2} \dots (\xi_1^N|b_1\rangle - \xi_2^N|b_2\rangle)_{b^N}] \\ &\quad \otimes [|+1\rangle_3\alpha_1|F\rangle_a (\delta_1^1|F\rangle + \delta_2^1|S\rangle)_{b^1} (\delta_1^2|F\rangle + \delta_2^2|S\rangle)_{b^2} \dots \\ &\quad (\delta_1^N|F\rangle + \delta_2^N|S\rangle)_{b^N} + |-1\rangle_3\alpha_2|S\rangle_a (\delta_1^1|F\rangle - \delta_2^1|S\rangle)_{b^1} (\delta_1^2|F\rangle \\ &\quad - \delta_2^2|S\rangle)_{b^2} \dots (\delta_1^N|F\rangle - \delta_2^N|S\rangle)_{b^N}], \end{aligned} \quad (18)$$

where $P = r_1'(r_2 - r_2')^3/8$.

Finally, after some classical feed-forward operations based on the measurements on the three NV centers in the orthogonal basis $\{|\pm\rangle\}$ according to **Table 1**, the system consisting of the control photon and target photons is projected into the state

$$\begin{aligned} |\Phi^N\rangle_4 &= P^{1+N} \times [\beta_1|\omega_1\rangle_a (\eta_1^1|\omega_1\rangle + \eta_2^1|\omega_2\rangle)_{b^1} (\eta_1^2|\omega_1\rangle \\ &\quad + \eta_2^2|\omega_2\rangle)_{b^2} \dots (\eta_1^N|\omega_1\rangle + \eta_2^N|\omega_2\rangle)_{b^N} + \beta_2|\omega_2\rangle_a (\eta_1^1|\omega_1\rangle \\ &\quad - \eta_2^1|\omega_2\rangle)_{b^1} (\eta_2^N|\omega_1\rangle - \eta_2^N|\omega_2\rangle)_{b^2} \dots (\eta_1^N|\omega_1\rangle \\ &\quad - \eta_2^N|\omega_2\rangle)_{b^N}] \otimes [\gamma_1|a_1\rangle_a (\xi_1^1|b_1\rangle + \xi_2^1|b_2\rangle)_{b^1} (\xi_1^2|b_1\rangle \\ &\quad + \xi_2^2|b_2\rangle)_{b^2} \dots (\xi_1^N|b_1\rangle + \xi_2^N|b_2\rangle)_{b^N} + \gamma_2|a_2\rangle_a (\xi_1^1|b_1\rangle \\ &\quad - \xi_2^1|b_2\rangle)_{b^1} (\xi_2^2|b_1\rangle - \xi_2^2|b_2\rangle)_{b^2} \dots (\xi_1^N|b_1\rangle - \xi_2^N|b_2\rangle)_{b^N}] \\ &\quad \otimes [\alpha_1|F\rangle_a (\delta_1^1|F\rangle + \delta_2^1|S\rangle)_{b^1} (\delta_1^2|F\rangle + \delta_2^2|S\rangle)_{b^2} \dots \\ &\quad (\delta_1^N|F\rangle + \delta_2^N|S\rangle)_{b^N} - \alpha_2|S\rangle_a (\delta_1^1|F\rangle - \delta_2^1|S\rangle)_{b^1} (\delta_1^2|F\rangle \\ &\quad - \delta_2^2|S\rangle)_{b^2} \dots (\delta_1^N|F\rangle - \delta_2^N|S\rangle)_{b^N}]. \end{aligned} \quad (19)$$

From **Eq. 19**, one can see that for each target photon b^n , phase flips take place on the frequency state $|\omega_2\rangle_{b^n}$, the spatial-mode state $|b_2\rangle_{b^n}$, and the polarization state $|S\rangle_{b^n}$ respectively when the

TABLE 2 | The relations between the measurement results on the three NV centers and the parity of the quantum state in the frequency, spatial-mode, and polarization DOFs, respectively.

Measurement	DOF	Parity	State
$ +\rangle_1$	frequency	even	$\beta_1\eta_1 \omega_1\rangle_a \omega_1\rangle_b + \beta_2\eta_2 \omega_2\rangle_a \omega_2\rangle_b$
$ -\rangle_1$	frequency	odd	$\beta_1\eta_2 \omega_1\rangle_a \omega_2\rangle_b + \beta_2\eta_1 \omega_2\rangle_a \omega_1\rangle_b$
$ +\rangle_2$	spatial mode	even	$\gamma_1\xi_1 a_1\rangle_a b_1\rangle_b + \gamma_2\xi_1 a_2\rangle_a b_2\rangle_b$
$ -\rangle_2$	spatial mode	odd	$\gamma_1\xi_2 a_1\rangle_a b_2\rangle_b + \gamma_2\xi_1 a_2\rangle_a b_1\rangle_b$
$ +\rangle_3$	polarization	even	$\alpha_1\delta_1 F\rangle_a F\rangle_b + \alpha_2\delta_2 S\rangle_a S\rangle_b$
$ -\rangle_3$	polarization	odd	$\alpha_1\delta_2 F\rangle_a S\rangle_b + \alpha_2\delta_1 S\rangle_a F\rangle_b$

frequency, the spatial-mode, and the polarization state of the control photon a is $|\omega_2\rangle_a$, $|a_2\rangle_a$, and $|S\rangle_a$. Meanwhile, from Eq. 19, one can see that there is only a global coefficient between the ideal desired output state and the realistic output state, which means the hyperparallel CPF^N is implemented with a robust fidelity to the realistic NV-cavity parameters. Overall, the quantum circuit is generalized to complete the high-fidelity photonic three-DOF hyperparallel CPF^N gate working on a multiple-photon system.

The quantum circuit shown in Figure 2 can be additionally generalized to implement a high-fidelity hyperparallel quantum parity-check gate in the polarization, frequency, and spatial-mode DOFs. Suppose photon a and photon b are initially prepared in the states $|\phi\rangle_a$ and $|\phi\rangle_b$ respectively. To check the parities of the two-photon states in three DOFs, the three NV centers are all initially prepared in the states $|+\rangle$, and the two photons are injected into the quantum circuit as shown in Figure 2 in sequence. If there is a click of the single-photon detectors while either of the photons passes through the quantum circuit, the process of the parity check is terminated. Otherwise, the state of the whole system consisting of two photons and three NV centers is transformed into the state

$$\begin{aligned}
 |\Phi^P\rangle = & \frac{r_1'^2(r_2 - r_2')^6}{64} [|+\rangle_1 (\beta_1\eta_1|\omega_1\rangle_a|\omega_1\rangle_b + \beta_2\eta_2|\omega_2\rangle_a|\omega_2\rangle_b) \\
 & + |-\rangle_1 (\beta_1\eta_2|\omega_1\rangle_a|\omega_2\rangle_b + \beta_2\eta_1|\omega_2\rangle_a|\omega_1\rangle_b)] \otimes [|+\rangle_2 \\
 & (\gamma_1\xi_1|a_1\rangle_a|b_1\rangle_b + \gamma_2\xi_1|a_2\rangle_a|b_2\rangle_b) + |-\rangle_2 (\gamma_1\xi_2|a_1\rangle_a|b_2\rangle_b) \\
 & + \gamma_2\xi_1|a_2\rangle_a|b_1\rangle_b] \otimes [|+\rangle_3 (\alpha_1\delta_1|F\rangle_a|F\rangle_b) \\
 & + \alpha_2\delta_2|S\rangle_a|S\rangle_b + |-\rangle_3 (\alpha_1\delta_2|F\rangle_a|S\rangle_b + \alpha_2\delta_1|S\rangle_a|F\rangle_b)].
 \end{aligned} \quad (20)$$

Therefore, after the three NV centers are measured in basis $\{| \pm \rangle\}$, the parities of the two-photon states in three DOFs can be obtained as shown in Table 2.

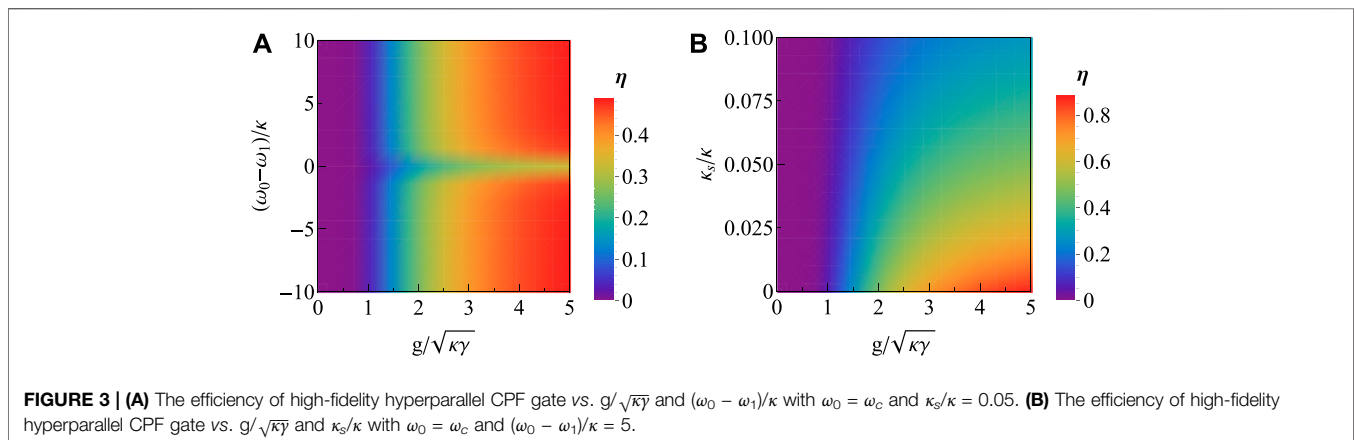
5 DISCUSSION AND SUMMARY

We have detailed the construction process of the photonic three-DOF hyperparallel CPF gate as shown in Figure 2, which can also be generalized to implement the photonic three-DOF hyperparallel CPF^N gate and parity-check gate. Meanwhile, we have shown that in the nearly realistic condition, the error items do not appear in the final output states and the difference between the ideal desired output states and the practical ones is only a global coefficient, as shown in Eqs 13, 19, 20. That is to say, these gates work with fidelities robust to the realistic NV-cavity parameters including g , γ , κ , and κ_s . In what follows, we quantitatively characterize the efficiency of the high-fidelity photonic three-DOF hyperparallel CPF gate, which is obtained as

$$\eta = \left| \frac{r_1'^2(r_2 - r_2')^6}{64} \right|. \quad (21)$$

Based on Eq. 21, the numerical simulation results are shown in Figure 3A and Figure 3B, where the efficiency is respectively treated as the function of $g/\sqrt{\kappa\gamma}$ and $(\omega_0 - \omega_1)/\kappa$ with $\kappa_s/\kappa = 0.05$ and $\omega_2 = \omega_0 = \omega_c$, and the function of $g/\sqrt{\kappa\gamma}$ and κ_s/κ with $(\omega_0 - \omega_1)/\kappa = 5$ and $\omega_2 = \omega_0 = \omega_c$. From Figure 3, one can see that the efficiency is much more sensitive to the variations of $g/\sqrt{\kappa\gamma}$ and κ_s/κ compared with the variation of $(\omega_0 - \omega_1)/\kappa$. An optical coupling of a NV center to an on-chip microcavity with the parameters $[g, \kappa, \gamma_{total}, \gamma_{ZPL}]/2\pi = [0.3, 26, 0.013, 0.0004]$ GHz has been demonstrated in the experiment [55]. Based on these experimental parameters, the efficiency $\eta = 38.51\%$ can be obtained provided $\kappa_s/\kappa = 0.05$ and $(\omega_0 - \omega_1)/\kappa = 5$. The efficiency is sacrificed for the high fidelity. That is to say, the computation errors are turned into detectable photon losses, which is advantageous for quantum computation.

The fidelities of the present photonic three-DOF hyperparallel gates are robust to the realistic NV-cavity parameters. In a more



generally realistic condition, some other factors effecting the fidelities should be evaluated, one of which is the mixture of the excited states of NV centers. A degree of mixing among the excited states of NV centers comes from a relatively low strain which is induced by the fabrication of optical resonators, and it would lead to an imperfect dipolar transition between the excited state and the ground state which is the interaction unit in our protocol. Fortunately, the excited state $|A_2\rangle$ is robust to the low strain and magnetic fields owing to the stable symmetric properties, and the mixing between the state $|A_2\rangle$ and the other excited states is very tiny in the low-strain regime, as demonstrated in the experiment implemented by Togan et al. [72], where small number ε is used to describe the imperfect dipolar transition between the excited state and the ground state $|+1\rangle$ induced by the low strain. It has been figured out that in the case $\varepsilon = 0.12$ (0.08), the fidelity of the interaction between the NV center in the state $|+1\rangle$ and the polarized photon in the state $|F\rangle = (|R\rangle + |L\rangle)/\sqrt{2}$ reaches 0.9928 (0.9968), which shows that the effect of the low strain on the fidelity of the interaction can be ignored [58]. Another factor of degrading the fidelity is the finite zero phonon line (ZPL) emission, which is relevant to the emitted photons from NV centers. In 2009, Barclay et al. [55] showed that it is possible to enhance the ZPL emission rate $\gamma_{ZPL}/\gamma_{total}$ by 47% if the Q value of the microdisk can be increased to 2.5×10^4 . In recent years, several techniques have been proposed which can enhance the ZPL emission rate $\gamma_{ZPL}/\gamma_{total}$ from 3% to 70% [75–79]. In addition, the fidelity is slightly lowered by errors in readout, spin preparation, spin decoherence, spin operation, spin flips during the process [80]. And the impact from the intracavity loss and linear optical elements loss [26, 34] should be considered. However, these limitations caused by the technical imperfections are not fundamental and can be largely improved with the further technical advances. For example, the spin-coherence time can achieve millisecond level in isotopically purified diamond [46] or by utilizing dynamical decoupling techniques [47, 48]. Moreover, Dolde et al. [50] realized the single electron spin operation with the fidelity $F \approx 0.99$ by utilizing engineered microwave pulses, and Fuchs et al. [49] reduced the manipulation time to the order of nanosecond.

We encode qubits in three DOFs including the polarization and spatial-mode and frequency DOFs of a two-photon system to complete our high-fidelity hyperparallel CPF gate, which further expands the capability of parallel computation compared with the ones working with one or two DOFs. The polarization and spatial-mode DOFs can be skillfully manipulated in experiment where arbitrary single-qubit operations on them are completed with linear optical elements, such as beam splitters, (circular) polarization beam splitters, phase shifter, and half-wave or quarter-wave plates. Frequency DOF has the advantages of large information capacity, highly nonlocal properties, and compatibility with current fiber optic technology infrastructure [81].

Extraordinary experimental and theoretical progress has been made on the frequency-encoded photonic qubits, such as the designation of the optical devices used to perform operations on the frequency-encoded photons [82, 83], the demonstration on coherent interference of frequency-encoded photons [84–88], the schemes of quantum gate for frequency qubits [42, 89], and the realization of discrete-frequency-entangled states [90]. In our protocol, the optical devices, including WDM for dividing photon with different frequencies from one path to different paths or completing the reverse conversion and FS for shifting the frequency, are utilized to manipulate frequencies and they are experimentally available. The WDM can be realized with Fiber Bragg Grating [91, 92], optical cavity [93, 94], or asymmetric Mach-Zehnder on the frequency encoding [95, 96]. The FS can be obtained by means of frequency up-conversion or down-conversion process [97–101].

In summary, we have proposed the approach for implementing the high-fidelity hyperparallel CPF gate working with the polarization, spatial-mode, and frequency DOFs of the two-photon system. The hyperparallel CPF gate works in the self-error-corrected pattern where the clicks of the single photon detectors remind the errors induced by the practical interaction and terminate the construction of the gate. Accordingly, the self-error-corrected pattern guarantees the realistic output state against the computation errors coming from practical interaction, enables the gate to work with high fidelity, and relaxes the current experimental requirement. In addition, the method can be generalized to implement high-fidelity photonic three-DOF hyperparallel CPF^N gate and parity-check gate. Maybe these features make this work useful in the hyperparallel quantum computation.

DATA AVAILABILITY STATEMENT

The original contributions presented in the study are included in the article/Supplementary material, further inquiries can be directed to the corresponding author.

AUTHOR CONTRIBUTIONS

G-YW: Conceptualization, Methodology, Validation, Writing-Original Draft, Writing-Review and Editing. H-RW: Conceptualization, Methodology, Validation, Writing-Review and Editing.

FUNDING

This work is supported by the National Natural Science Foundation of China under Grant No. 12004029 and the Fundamental Research Funds for the Central Universities under Grant No. FRF-TP-19-011A3.

REFERENCES

- Nielsen MA, Chuang IL. *Quantum Computation and Quantum Information*. Cambridge, UK: Cambridge University Press (2000).
- Bennett CH, Brassard G, Crépeau C, Jozsa R, Peres A, Wootters WK. Teleporting an Unknown Quantum State via Dual Classical and Einstein-Podolsky-Rosen Channels. *Phys Rev Lett* (1993) 70:1895–9. doi:10.1103/physrevlett.70.1895
- Bennett CH, Wiesner SJ. Communication via One- and Two-Particle Operators on Einstein-Podolsky-Rosen States. *Phys Rev Lett* (1992) 69:2881–4. doi:10.1103/physrevlett.69.2881
- Liu XS, Long GL, Tong DM, Li F. General Scheme for Superdense Coding between Multiparties. *Phys Rev A* (1992) 65:022304. doi:10.1103/physreva.65.022304
- Ekert AK. Quantum Cryptography Based on Bell's Theorem. *Phys Rev Lett* (1991) 67:661–3. doi:10.1103/physrevlett.67.661
- Bennett CH, Brassard G, Mermin ND. Quantum Cryptography without Bell's Theorem. *Phys Rev Lett* (1992) 68:557–9. doi:10.1103/physrevlett.68.557
- Hillery M, Bužek V, Berthiaume A. Quantum Secret Sharing. *Phys Rev A* (1999) 59:1829–34. doi:10.1103/physreva.59.1829
- Long GL, Liu XS. Theoretically Efficient High-Capacity Quantum-Key-Distribution Scheme. *Phys Rev A* (2002) 65:032302. doi:10.1103/physreva.65.032302
- Deng FG, Long GL, Liu XS. Two-step Quantum Direct Communication Protocol Using the Einstein-Podolsky-Rosen Pair Block. *Phys Rev A* (2003) 68:042317. doi:10.1103/physreva.68.042317
- Zhang W, Ding DS, Sheng YB, Zhou L, Shi BS, Guo GC. Quantum Secure Direct Communication with Quantum Memory. *Phys Rev Lett* (2007) 118:220501. doi:10.1103/PhysRevLett.118.220501
- Liu B, Xia S, Xiao D, Huang W, Xu B, Li Y. Decoy-state Method for Quantum-Key-Distribution-Based Quantum Private Query. *Sci China Phys Mech Astron* (2022) 65:240312. doi:10.1007/s11433-021-1843-7
- Lv S-X, Jiao X-F, Zhou P. Multiparty Quantum Computation for Summation and Multiplication with Mutually Unbiased Bases. *Int J Theor Phys* (2019) 58:2872–82. doi:10.1007/s10773-019-04170-z
- Zhou L, Sheng Y-B. One-step Device-independent Quantum Secure Direct Communication. *Sci China Phys Mech Astron* (2022) 65:250311. doi:10.1007/s11433-021-1863-9
- Li Z, Wei K. Improving Parameter Optimization in Decoy-State Quantum Key Distribution. *Quan Eng* (2022) 2022:9717591. doi:10.1155/2022/9717591
- Shor PW. Algorithms for Quantum Computation: Discrete Logarithms and Factoring. In: Goldwasser S, editor. Proceedings 35th annual Symposium on Foundations Of Computer Science; 1994 Nov 20–22; Santa Fe, NM. IEEE (1994). p. 124–34.
- Grover LK. Quantum Mechanics Helps in Searching for a Needle in a Haystack. *Phys Rev Lett* (1997) 79:325–8. doi:10.1103/physrevlett.79.325
- Long GL. Grover Algorithm with Zero Theoretical Failure Rate. *Phys Rev A* (2001) 64:022307. doi:10.1103/physreva.64.022307
- Xu GF, Tong DM. Realizing Multi-Qubit Controlled Nonadiabatic Holonomic gates with Connecting Systems. *AAPPS Bull* (2022) 32:13. doi:10.1007/s43673-022-00043-6
- Giovannetti V, Lloyd S, Maccone L. Quantum-enhanced Measurements: Beating the Standard Quantum Limit. *Science* (2004) 306:1330–6. doi:10.1126/science.1104149
- Cai X-D, Wu D, Su Z-E, Chen M-C, Wang X-L, Li L, et al. Entanglement-based Machine Learning on a Quantum Computer. *Phys Rev Lett* (2015) 114:110504. doi:10.1103/physrevlett.114.110504
- Allcock J, Zhang S. Quantum Machine Learning. *Natl Sci Rev* (2019) 6:26–8. doi:10.1093/nsr/nw1149
- Ouyang XL, Huang XZ, Wu YK, Zhang WG, Wang X, Zhang HL, et al. Experimental Demonstration of Quantum-Enhanced Machine Learning in a Nitrogen-Vacancy-center System. *Phys Rev A* (2020) 101:012307. doi:10.1103/physreva.101.012307
- Zhang N-N, Tao M-J, He W-T, Chen X-Y, Kong X-Y, Deng F-G, et al. Efficient Quantum Simulation of Open Quantum Dynamics at Various Hamiltonians and Spectral Densities. *Front Phys* (2021) 16:51501. doi:10.1007/s11467-021-1064-y
- Wang B-X, Tao M-J, Ai Q, Xin T, Lambert N, Ruan D, et al. Efficient Quantum Simulation of Photosynthetic Light Harvesting. *Npj Quan Inf* (2018) 4:52. doi:10.1038/s41534-018-0102-2
- Barenco A, Bennett CH, Cleve R, DiVincenzo DP, Margolus N, Shor P, et al. Elementary gates for Quantum Computation. *Phys Rev A* (1995) 52:3457–67. doi:10.1103/physreva.52.3457
- Reiserer A, Kalb N, Rempe G, Ritter S. A Quantum Gate between a Flying Optical Photon and a Single Trapped Atom. *Nature* (2014) 508:237–40. doi:10.1038/nature13177
- Tiecke TG, Thompson JD, de Leon NP, Liu LR, Vuletić V, Lukin MD. Nanophotonic Quantum Phase Switch with a Single Atom. *Nature* (2014) 508:241–4. doi:10.1038/nature13188
- Ren Bao-Cang BC, Deng Fu-Guo FG. Hyper-parallel Photonic Quantum Computation and Manipulation on Hyperentangled States. *Acta Phys Sin* (2015) 64:160303. doi:10.7498/aps.64.160303
- Ren B-C, Wei H-R, Deng F-G. Deterministic Photonic Spatial-Polarization Hyper-Controlled-Not Gate Assisted by a Quantum Dot inside a One-Side Optical Microcavity. *Laser Phys Lett* (2013) 10:095202. doi:10.1088/1612-2011/10/9/095202
- Ren BC, Wang GY, Deng FG. Universal Hyperparallel Hybrid Photonic Quantum gates with Dipole-Induced Transparency in the Weak-Coupling Regime. *Phys Rev A* (2015) 91:032328. doi:10.1103/physreva.91.032328
- Ren B-C, Deng F-G. Hyper-parallel Photonic Quantum Computation with Coupled Quantum Dots. *Sci Rep* (2014) 4:4623. doi:10.1038/srep04623
- Li T, Long GL. Hyperparallel Optical Quantum Computation Assisted by Atomic Ensembles Embedded in Double-Sided Optical Cavities. *Phys Rev A* (2016) 94:022343. doi:10.1103/physreva.94.022343
- Wang T-J, Zhang Y, Wang C. Universal Hybrid Hyper-Controlled Quantum gates Assisted by Quantum Dots in Optical Double-Sided Microcavities. *Laser Phys Lett* (2014) 11:025203. doi:10.1088/1612-2011/11/2/025203
- Wei H-R, Deng F-G, Long GL. Hyper-parallel Toffoli Gate on Three-Photon System with Two Degrees of freedom Assisted by Single-Sided Optical Microcavities. *Opt Express* (2016) 24:18619–30. doi:10.1364/oe.24.018619
- Ren B-C, Wang AH, Alsaedi A, Hayat T, Deng F-G. Three-photon Polarization-Spatial Hyperparallel Quantum Fredkin Gate Assisted by diamond Nitrogen Vacancy center in Optical Cavity. *Annalen Der Physik* (2018) 530:1800043. doi:10.1002/andp.201800043
- Wei HR, Liu WQ, Chen NY. Implementing a Two-Photon Three-Degrees-of-Freedom Hyper-Parallel Controlled Phase Flip Gate through Cavity-Assisted Interactions. *Annalen Der Physik* (2020) 532:1900578. doi:10.1002/andp.201900578
- Marrucci L, Manzo C, Paparo D. Optical Spin-To-Orbital Angular Momentum Conversion in Inhomogeneous Anisotropic media. *Phys Rev Lett* (2006) 96:163905. doi:10.1103/physrevlett.96.163905
- Nagali E, Sciarrino F, De Martini F, Marrucci L, Piccirillo B, Karimi E, et al. Quantum Information Transfer from Spin to Orbital Angular Momentum of Photons. *Phys Rev Lett* (2009) 103:013601. doi:10.1103/PhysRevLett.103.013601
- Pinheiro ARC, Souza CER, Caetano DP, Huguenin JAO, Schmidt AGM, Khoury AZ. Vector Vortex Implementation of a Quantum Game. *J Opt Soc Am B* (2013) 30:3210–4. doi:10.1364/josab.30.003210
- Milione G, Nguyen TA, Leach J, Nolan DA, Alfano RR. Using the Nonseparability of Vector Beams to Encode Information for Optical Communication. *Opt Lett* (2015) 40:4887–90. doi:10.1364/ol.40.004887
- Balthazar WF, Souza CER, Caetano DP, Galvão EF, Huguenin JAO, Khoury AZ. Tripartite Nonseparability in Classical Optics. *Opt Lett* (2016) 41:5797–800. doi:10.1364/ol.41.005797
- Lu HH, Lukens JM, Williams BP, Imany P, Peters NA, Weiner AM, et al. A Controlled-NOT Gate for Frequency-Bin Qubits. *Npj Quan Inf* (2019) 5:5797–800. doi:10.1038/s41534-019-0137-z
- Zeng Z, Zhu K-D. Complete Hyperentangled Bell State Analysis Assisted by Hyperentanglement. *Laser Phys Lett* (2020) 17:075203. doi:10.1088/1612-202x/ab9117
- Jelezko F, Gaebel T, Popa I, Gruber A, Wrachtrup J. Observation of Coherent Oscillations in a Single Electron Spin. *Phys Rev Lett* (2004) 92:076401. doi:10.1103/PhysRevLett.92.076401

45. Childress L, Gurudev Dutt MV, Taylor JM, Zibrov AS, Jelezko F, Wrachtrup J, et al. Coherent Dynamics of Coupled Electron and Nuclear Spin Qubits in diamond. *Science* (2006) 314:281–5. doi:10.1126/science.1131871
46. Balasubramanian G, Neumann P, Twitchen D, Markham M, Kolesov R, Mizuochi N, et al. Ultralong Spin Coherence Time in Isotopically Engineered diamond. *Nat Mater* (2009) 8:383–7. doi:10.1038/nmat2420
47. Naydenov B, Dolde F, Hall LT, Shin C, Fedder H, Hollenberg LCL, et al. Dynamical Decoupling of a Single-Electron Spin at Room Temperature. *Phys Rev B* (2011) 83:081201. doi:10.1103/physrevb.83.081201
48. de Lange G, Wang ZH, Risté D, Dobrovitski VV, Hanson R. Universal Dynamical Decoupling of a Single Solid-State Spin from a Spin bath. *Science* (2010) 330:60–3. doi:10.1126/science.1192739
49. Fuchs GD, Dobrovitski VV, Toyli DM, Heremans FJ, Awschalom DD. Gigahertz Dynamics of a Strongly Driven Single Quantum Spin. *Science* (2009) 326:1520–2. doi:10.1126/science.1181193
50. Dolde F, Bergholm V, Wang Y, Jakobi I, Naydenov B, Pezzagna S, et al. High-fidelity Spin Entanglement Using Optimal Control. *Nat Commun* (2014) 5:3371. doi:10.1038/ncomms4371
51. Robledo L, Childress L, Bernien H, Hensen B, Alkemade PFA, Hanson R. High-fidelity Projective Read-Out of a Solid-State Spin Quantum Register. *Nature* (2011) 477:574–8. doi:10.1038/nature10401
52. Holzgrafe J, Beitner J, Kara D, Knowles HS, Atatüre M. Error Corrected Spin-State Readout in a Nanodiamond. *Npj Quan Inf* (2019) 5:13. doi:10.1038/s41534-019-0126-2
53. Park Y-S, Cook AK, Wang H. Cavity QED with diamond Nanocrystals and Silica Microspheres. *Nano Lett* (2006) 6:2075–9. doi:10.1021/nl061342r
54. Barbour RJ, Dinyari KN, Wang H. A Composite Microcavity of diamond Nanopillar and Deformed Silica Microsphere with Enhanced Evanescent Decay Length. *Opt Express* (2010) 18:18968–74. doi:10.1364/oe.18.018968
55. Barclay PE, Fu K-MC, Santori C, Beausoleil RG. Chip-based Microcavities Coupled to Nitrogen-Vacancy Centers in Single crystal diamond. *Appl Phys Lett* (2009) 95:191115. doi:10.1063/1.3262948
56. Chen Q, Yang WL, Feng M, Du JF. Entangling Separate Nitrogen-Vacancy Centers in a Scalable Fashion via Coupling to Microtoroidal Resonators. *Phys Rev A* (2011) 83:054305. doi:10.1103/physreva.83.054305
57. Wei HR, Deng FG. Compact Quantum gates on Electron-Spin Qubits Assisted by diamond Nitrogen-Vacancy Centers inside Cavities. *Phys Rev A* (2013) 88:042323. doi:10.1103/physreva.88.042323
58. Wang TJ, Wang C. Universal Hybrid Three-Qubit Quantum gates Assisted by a Nitrogen-Vacancy center Coupled with a Whispering-Gallery-Mode Microresonator. *Phys Rev A* (2014) 90:052310. doi:10.1103/physreva.90.052310
59. Wei H-R, Lu Long G. Hybrid Quantum gates between Flying Photon and diamond Nitrogen-Vacancy Centers Assisted by Optical Microcavities. *Sci Rep* (2015) 5:12918. doi:10.1038/srep12918
60. Li Y, Aolita L, Chang DE, Kwek LC. Robust-fidelity Atom-Photon Entangling gates in the Weak-Coupling Regime. *Phys Rev Lett* (2012) 109:160504. doi:10.1103/physrevlett.109.160504
61. Borregaard J, Kómár P, Kessler EM, Sørensen AS, Lukin MD. Heralded Quantum gates with Integrated Error Detection in Optical Cavities. *Phys Rev Lett* (2015) 114:110502. doi:10.1103/physrevlett.114.110502
62. Li T, Deng FG. Error-rejecting Quantum Computing with Solid-State Spins Assisted by Low-Q Optical Microcavities. *Phys Rev A* (2016) 94:062310. doi:10.1103/physreva.94.062310
63. Qin W, Wang X, Miranowicz A, Zhong Z, Nori F. Heralded Quantum Controlled-phase gates with Dissipative Dynamics in Macroscopically Distant Resonators. *Phys Rev A* (2017) 96:012315. doi:10.1103/physreva.96.012315
64. Ren B-C, Deng F-G. Robust Hyperparallel Photonic Quantum Entangling Gate with Cavity QED. *Opt Express* (2017) 25:10863–73. doi:10.1364/oe.25.101863
65. Shapira Y, Shaniv R, Manovitz T, Akerman N, Ozeri R. Robust Entanglement gates for Trapped-Ion Qubits. *Phys Rev Lett* (2018) 121:180502. doi:10.1103/physrevlett.121.180502
66. Wang G-Y, Li T, Ai Q, Deng F-G. Self-error-corrected Hyperparallel Photonic Quantum Computation Working with Both the Polarization and the Spatial-Mode Degrees of freedom. *Opt Express* (2018) 26:23333–46. doi:10.1364/oe.26.023333
67. Li M, Zhang M. Robust Universal Photonic Quantum gates Operable with Imperfect Processes Involved in diamond Nitrogen-Vacancy Centers inside Low-Q Single-Sided Cavities. *Opt Express* (2018) 26:33129–41. doi:10.1364/oe.26.033129
68. Li M, Lin J-Y, Zhang M. High-fidelity Hybrid Quantum gates between a Flying Photon and diamond Nitrogen-Vacancy Centers Assisted by Low-Q Single-Sided Cavities. *Annalen Der Physik* (2019) 531:1800312. doi:10.1002/andp.201800312
69. Wei H-R, Zheng Y-B, Hua M, Xu G-F. Robust-fidelity Hyperparallel Controlled-Phase-Flip Gate through Microcavities. *Appl Phys Express* (2020) 13:082007. doi:10.35848/1882-0786/aba64a
70. Xu Y, Chu J, Yuan J, Qiu J, Zhou Y, Zhang L, et al. High-fidelity, High-Scalability Two-Qubit Gate Scheme for Superconducting Qubits. *Phys Rev Lett* (2020) 125:240503. doi:10.1103/physrevlett.125.240503
71. Han Y-H, Cao C, Fan L, Zhang R. Heralded High-Fidelity Quantum Hyper-CNOT gates Assisted by Charged Quantum Dots inside Single-Sided Optical Microcavities. *Opt Express* (2021) 29:20045–62. doi:10.1364/oe.426325
72. Togan E, Chu Y, Trifonov AS, Jiang L, Maze J, Childress L, et al. Quantum Entanglement between an Optical Photon and a Solid-State Spin Qubit. *Nature* (2010) 466:730–4. doi:10.1038/nature09256
73. An JH, Feng M, Oh CH. Quantum-information Processing with a Single Photon by an Input-Output Process with Respect to Low-Q Cavities. *Phys Rev A* (2009) 79:032303. doi:10.1103/physreva.79.032303
74. Hu CY, Young A, O'Brien JL, Munro WJ, Rarity JG. Giant Optical Faraday Rotation Induced by a Single-Electron Spin in a Quantum Dot: Applications to Entangling Remote Spins via a Single Photon. *Phys Rev B* (2008) 78:085307. doi:10.1103/physrevb.78.085307
75. Kolesov R, Grotz B, Balasubramanian G, Stöhr RJ, Nicolet AAL, Hemmer PR, et al. Wave-particle Duality of Single Surface Plasmon Polaritons. *Nat Phys* (2009) 5:470–4. doi:10.1038/nphys1278
76. Schietinger S, Barth M, Aichele T, Benson O. Plasmon-Enhanced Single Photon Emission from a Nanoassembled Metal-Diamond Hybrid Structure at Room Temperature. *Nano Lett* (2009) 9:1694–8. doi:10.1021/nl900384c
77. Barclay PE, Fu KMC, Santori C, Faraon A, Beausoleil RG. Hybrid Nanocavity Resonant Enhancement of Color Center Emission in Diamond. *Phys Rev X* (2011) 1:011007. doi:10.1103/physrevx.1.011007
78. Faraon A, Barclay PE, Santori C, Fu K-MC, Beausoleil RG. Resonant Enhancement of the Zero-Phonon Emission from a Colour Centre in a Diamond Cavity. *Nat Photon* (2011) 5:301–5. doi:10.1038/nphoton.2011.52
79. Faraon A, Santori C, Huang Z, Acosta VM, Beausoleil RG. Coupling of Nitrogen-Vacancy Centers to Photonic Crystal Cavities in Monocrystalline Diamond. *Phys Rev Lett* (2012) 109:033604. doi:10.1103/PhysRevLett.109.033604
80. Bernien H, Hensen B, Pfaff W, Koolstra G, Blok MS, Robledo L, et al. Heralded Entanglement between Solid-State Qubits Separated by Three Metres. *Nature* (2013) 497:86–90. doi:10.1038/nature12016
81. Ou BQ, Liu C, Sun Y, Chen PX. Deterministically Swapping Frequency-Bin Entanglement from Photon-Photon to Atom-Photon Hybrid Systems. *Phys Rev A* (2018) 97:023839. doi:10.1103/physreva.97.023839
82. Lu HH, Lukens JM, Peters NA, Odele OD, Leaird DE, Weiner AM, et al. Electro-optic Frequency Beam Splitters and Tritters for High-Fidelity Photonic Quantum Information Processing. *Phys Rev Lett* (2018) 120:030502. doi:10.1103/PhysRevLett.120.030502
83. Hu YW, Yu MJ, Zhu D, Sinclair N, Shams-Ansari A, Shao LB, et al. On-chip Electro-Optic Frequency Shifters and Beam Splitters. *Nature* (2021) 599:7886. doi:10.1038/s41586-021-03999-x

84. Clemmen S, Farsi A, Ramelow S, Gaeta AL. Ramsey Interference with Single Photons. *Phys Rev Lett* (2016) 117:223601. doi:10.1103/physrevlett.117.223601
85. Kobayashi T, Ikuta R, Yasui S, Miki S, Yamashita T, Terai H, et al. Frequency-domain Hong-Ou-Mandel Interference. *Nat Photon* (2011) 10:441–4. doi:10.1038/nphoton.2016.74
86. Kobayashi T, Yamazaki D, Matsuki K, Ikuta R, Miki S, Yamashita T, et al. Mach-Zehnder Interferometer Using Frequency-Domain Beamsplitter. *Opt Express* (2017) 25:12052–60. doi:10.1364/oe.25.012052
87. Lu H-H, Lukens JM, Peters NA, Williams BP, Weiner AM, Lougovski P. Quantum Interference and Correlation Control of Frequency-Bin Qubits. *Optica* (2018) 5:1455–60. doi:10.1364/optica.5.001455
88. Imany P, Odele OD, Alshaykh MS, Lu H-H, Leaird DE, Weiner AM. Frequency-domain Hong-Ou-Mandel Interference with Linear Optics. *Opt Lett* (2018) 43:2760–3. doi:10.1364/ol.43.002760
89. Lukens JM, Lougovski P. Frequency-encoded Photonic Qubits for Scalable Quantum Information Processing. *Optica* (2017) 4:8–16. doi:10.1364/optica.4.000008
90. Ramelow S, Ratschbacher L, Fedrizzi A, Langford NK, Zeilinger A. Discrete Tunable Color Entanglement. *Phys Rev Lett* (2009) 103:253601. doi:10.1103/physrevlett.103.253601
91. Bloch M, McLaughlin SW, Merolla J-M, Patois F. Frequency-coded Quantum Key Distribution. *Opt Lett* (2007) 32:301–3. doi:10.1364/ol.32.000301
92. Zhang T, Yin Z-Q, Han Z-F, Guo G-C. A Frequency-Coded Quantum Key Distribution Scheme. *Opt Commun* (2008) 281:4800–2. doi:10.1016/j.optcom.2008.06.009
93. Huntington EH, Ralph TC. Separating the Quantum Sidebands of an Optical Field. *J Opt B Quan Semiclass. Opt.* (2002) 4:123–8. doi:10.1088/1464-4266/4/2/307
94. Zhang J. Einstein-Podolsky-Rosen Sideband Entanglement in Broadband Squeezed Light. *Phys Rev A* (2003) 67:054302. doi:10.1103/physreva.67.054302
95. Huntington EH, Ralph TC. Components for Optical Qubits Encoded in Sideband Modes. *Phys Rev A* (2004) 69:042318. doi:10.1103/physreva.69.042318
96. Huntington EH, Milford GN, Robilliard C, Ralph TC. Coherent Analysis of Quantum Optical Sideband Modes. *Opt Lett* (2005) 30:2481–3. doi:10.1364/ol.30.002481
97. Langrock C, Diamanti E, Roussev RV, Yamamoto Y, Fejer MM, Takesue H. Highly Efficient Single-Photon Detection at Communication Wavelengths by Use of Upconversion in Reverse-Proton-Exchanged Periodically Poled LiNbO₃ Waveguides. *Opt Lett* (2005) 30:1725–7. doi:10.1364/ol.30.001725
98. Takesue H, Diamanti E, Honjo T, Langrock C, Fejer MM, Inoue K, et al. Differential Phase Shift Quantum Key Distribution experiment over 105 Km Fibre *New J Phys* (2005) 7:232. doi:10.1088/1367-2630/7/1/232
99. Takesue H. Erasing Distinguishability Using Quantum Frequency Up-Conversion. *Phys Rev Lett* (2008) 101:173901. doi:10.1103/physrevlett.101.173901
100. Zhou Z-Y, Liu S-L, Li Y, Ding D-S, Zhang W, Shi S, et al. Orbital Angular Momentum-Entanglement Frequency Transducer. *Phys Rev Lett* (2016) 117:103601. doi:10.1103/physrevlett.117.103601
101. Ikuta R, Kusaka Y, Kitano T, Kato H, Yamamoto T, Koashi M, et al. Wide-band Quantum Interface for Visible-To-Telecommunication Wavelength Conversion. *Nat Commun* (2011) 2:537. doi:10.1038/ncomms1544

Conflict of Interest: The authors declare that the research was conducted in the absence of any commercial or financial relationships that could be construed as a potential conflict of interest.

Publisher's Note: All claims expressed in this article are solely those of the authors and do not necessarily represent those of their affiliated organizations, or those of the publisher, the editors and the reviewers. Any product that may be evaluated in this article, or claim that may be made by its manufacturer, is not guaranteed or endorsed by the publisher.

Copyright © 2022 Wang and Wei. This is an open-access article distributed under the terms of the Creative Commons Attribution License (CC BY). The use, distribution or reproduction in other forums is permitted, provided the original author(s) and the copyright owner(s) are credited and that the original publication in this journal is cited, in accordance with accepted academic practice. No use, distribution or reproduction is permitted which does not comply with these terms.